PARAMETRIC STUDY OF LAMINAR FREE CONVECTION IN INCLINED POROUS ANNULUS WITH FINS ON THE INNER CYLINDER

Dr. Saad M. AL-Mashaat
Ass. Prof. /University of Baghdad

Manal H. AL-Hafidh
Ass. Prof. /University of Baghdad

ABSTRACT

An experimental and numerical study has been carried out to investigate the heat transfer by natural convection in a three dimensional annulus enclosure filled with porous media (silica sand) between two inclined concentric cylinders with (and without) annular fins attached to the inner cylinder under steady state condition; The experiments were carried out for a range of modified Rayleigh number ($0.2 \leq Ra^* \leq 11$) and extended to $Ra^*=500$ for numerical study, annulus inclination angle of ($\delta = 0^\circ, 30^\circ, 60^\circ$ and 90°). The numerical study was to write the governing equation under an assumptions used Darcy law and Boussinesq's approximation and then solved numerically using finite difference approximation. It was found that the average Nusselt number depends on (Ra^*, Hf, δ and Rr) and the maximum value of the local Nusselt number for vertical cylinder is about two times as large as that of the horizontal case. The results showed that, increasing of fin length increases the heat transfer rate for any fins pitch unless the area of the inner cylinder exceeds that of the outer one, then the heat will be stored in the porous media. A correlation for Nu in terms of Ra, Rr and δ, has been developed for inner cylinder. A comparison was made between the results of the present work and with other researches for the case without fins and excellent agreement was obtained and reveals deviation less than 5 % for average Nusselt number.

دراسة إستدلالية للحمل الحر الطباقي في فجوة حلقية مملؤة بوسط مسامي مع زعانف على الأسطوانة الداخلية

الخلاصة:

أجريت في هذا البحث دراسة عملية ونظرية لإنتقال الطاقة الحرارية بالحمل الحر في فجوة حلقية ثلاثية الأبعاد مملؤة بوسط مسامي(رمل) بين أسطوانتين مائلتين متحدتي المركز بوجود (وعدم وجود) زعانف متصلة بالإسطوانة الداخلية تحت شروط حالة الإستقرار. أجريت التجارب العملية لمدى عدد رالي المعدل ($0.2 \leq Ra^* \leq 11$) ولمدى $Ra^*=500$ في الجزء النظري ولزاوية ميل ($\delta = 0^\circ, 30^\circ, 60^\circ$ and 90°). تم كتابة المعادلات الحاكمة في الدراسة النظرية تحت فرضيات قانون دارسي وتقريب بوسنسك وتحويلها الى معادلة بدلالة الجهد المتجه والتي بدورها حلت عدديا باستخدام طريقة الفروق المحددة. تتضمن إمكانية الحل العددي حساب الجهد المتجه ودرجة الحرارة وعدد نسلت الموقعي والمتوسط. بينت النتائج أن عدد نسلت المتوسط يعتمد على عدد رالي المعدل وطول الزعنفة وزاوية ميل الأسطوانة ونسبة الأقطار، وأن أقصى عدد نسلت الموقعي للأسطوانة العمودية حوالي الضعف لتلك في حالة الأسطوانة الأفقية. بينت النتائج أن زيادة طول الزعنفة لأي خطوة زعنفة يسبب زيادة في أنتقال الطاقة الحرارية إلا في حالة زيادة المساحة السطحية للأسطوانة الداخلية على تلك التي للأسطوانة الخارجية فإن ذلك يتسبب في خزن الطاقة الحرارية في الوسط المسامي. مثلت النتائج العملية والنظرية بمعادلات تجريبية للأسطوانة الداخلية تربط عدد نسلت الموقعي بعدد رالي المعدل ونسبة الأقطاروزاوية الميل. قورنت النتائج للبحث الحالي مع نتائج بحوث أخرى في حالة عدم وجود زعانف وأعطت توافق جيد بنسبة إنحراف 5% لعدد نسلت المتوسط.

KEY WORDS: natural convection, three dimensional, inclined annulus, porous media and annular fins

INTRODUCTION:

Recent advances in heat transfer and fluid mechanics, together with the development of large digital computers has made feasible the study of many natural phenomena of great practical importance. A case in point is the analysis of enclosure problem (free convection of a fluid in an annular container)

Also natural convection in porous annuli has a wide variety of technological applications such as the insulation of an aircraft cabin and thermal insulation of buildings or horizontal pipes, reactors, the storage of thermal energy, and underground cable systems, ground water flows oil recovery processes and geological of high – level nuclear waste, food processing, design of regenerative heat exchangers and solar energy collectors etc. representative reviews of these applications and other convective heat transfer applications in porous media may be found in the resent books and researches by **(Prasad et.al., 1985), (Prasad 1986), (Nield and Bejan, 1999) and (Taha et. al., 2004).**

A genetic algorithm was used by **(Giampietro, 2005)** to find the optimum profile of longitudinal convective heat dissipating fins located in a tube where a viscous fluid passes through in laminar flow. To this aim, velocity and temperature distributions in the finned tube were determined with the help of a finite element model, which took the effect of viscous dissipation into account. A global heat transfer coefficient was consequently calculated. After having assigned a polynomial lateral profile to the fins of the tube, the geometry was then optimized in order to maximize the heat transferred per unit of tube length respecting constraints on the tube weight or the pressure drop along the duct.

(Irfan et. al., 2006) investigated the steady state heat transfer in a porous medium fixed in a vertical annular cylinder. The Darcy model of flow is employed. The inner surface of the vertical annulus was maintained at constant wall temperature and the outer surface remains at ambient temperature and the heat transfer was assumed to take place by convection and radiation for Ra range (50 -200). The equations governing the flow behavior are solved using finite element method. The results show that when the radius ratio increased the isotherm of the fluid as well as solid phase move toward the hot surface and away from cold surface. It's found that the Nusselt number of the solid phase does not vary much with respect to aspect ratio ($0 < A < 10$) of the annulus when the inter phase heat transfer coefficient and the modified conductivity ratio is small. The Nusselt number of the fluid phase decrease with increase of the inter phase heat transfer coefficient whereas the Nusselt number of the solid increase with the increase of the inter phase heat transfer coefficient.

Natural convection heat transfer between two horizontal concentric cylinders with two fins attached to the inner cylinder was numerically investigated by **(Alshahrani and Zeitoun, 2007)** using finite element technique together with SIMPLER algorithm. Laminar conditions up to Rayleigh number Ra of 5×10^4 were investigated as well as effects of annulus diameter ratio, fin length and fin inclination angle on this type of flow. A conduction thermal resistance of finned annulus was obtained by means of conduction heat transfer analysis. The thermal

resistance decreases as fin length increases or as annulus diameter ratio decreases. Results of natural convection in finned annuli were presented in the forms of streamlines and isothermal plots. Data of heat transfer in annuli were presented in terms of Nusselt number and effective thermal conductivity ratio ke/k versus Rayleigh number.

To extend the existing studies, the parametric of the three dimensional laminar free convection in an inclined annulus with porous media and with (and without) fins attached to the inner cylinder will be addressed.

EXPERIMENTAL STUDY

Three outer cylinders of different diameters was manufactured to vary the radius ratio and to vary fin length, ten inner cylinders was manufactured one without fins and others with different fin length(Hf =3mm, 7mm and 11mm), radius ratios of ($Rr=(r_1/r_2)$ = 0.293, 0.364 and 0.435), number of fins (n=12, 23 and 45) and pitch length of (s = 19.2mm, 8.4mm and 3mm) to investigate the effect of these parameters and the effect of modified Rayleigh number by the variation of the temperature difference between the two concentric cylinders by means of a variable electric input power. Aluminum was chosen due to its high thermal conductivity and easy machinability. The test section consists of a three Aluminum outer cylinders of (100 mm), (82 mm) and (70 mm) outside diameters, (4 mm) thick and (260mm) long to which ten Aluminum inner cylinders of (27mm) outside diameter, (260 mm) long and (5 mm) thick. The inner cylinder was heated by passing an alternating current to a heater inside the inner cylinder and the outer cylinder was subjected to the surrounding temperature (freezer) where the minimum temperature was 270 K. The inner cylinder surface temperatures were measured at six locations using thermocouples type K.

MATHEMATICAL MODEL

The schematic drawing of the geometry and the Cartesian coordinate system employed in solving the problem is shown in **Fig.1.**

In order to model the incompressible flow in the porous medium, the steady-state equations of the Darcy flow model, namely, the mass, the momentum (Darcy), the energy conservation laws and the Boussinesq's approximation are employed. These equations in vectorial notation are given by **(Nield and Bejan 1999)** and fin equation by **(Ramón and Sergio, 2007).**

Governing Equations

The conservation equations of mass, momentum and energy in steady state and the supplementary equation are:

$$\rho = \rho_2 \{1 - \beta(T - T_2)\} \quad (1)$$

Where:

$$\beta = \frac{1}{\rho}\frac{\partial \rho}{\partial T} \quad (2)$$

β Is the thermal coefficient of the volume expansion, this constant is evaluated at T_2 which is the temperature at the inner surface of the outer cylinder, ρ_2 is the density at T_2 and ρ is the density at T, **(Fukuda et. al.1980)**. This technique is called Boussinesq's approximation.

Mass Conservation

$$\frac{\partial u_r}{\partial r} + \frac{u_r}{r} + \frac{1}{r}\frac{\partial u_\phi}{\partial \phi} + \frac{\partial u_z}{\partial z} = 0 \quad (3)$$

Momentum Equations

The most common model used for flow in the porous media is the Darcy flow model. Darcy's law states that the volume average velocity through the porous material is proportional with the pressure gradient. In three dimensional flows, the Darcy's model **(Wang and Zhang 1990)** is:

Momentum Equation In Radial Direction

$$u_r = \frac{K}{\mu_f}\left[-\frac{\partial p}{\partial r} - \rho\, g\, \cos\phi\, \cos\delta\right] \tag{4}$$

Momentum Equation In Angular Direction

$$u_\phi = \frac{K}{\mu_f}\left[-\frac{1}{r}\frac{\partial p}{\partial \phi} + \rho\, g\, \sin\phi\, \cos\delta\right] \tag{5}$$

Momentum Equation In Axial Direction

$$u_z = \frac{K}{\mu_f}\left[-\frac{\partial p}{\partial z} - \rho\, g\, \sin\delta\right] \tag{6}$$

Energy Equation

$$\frac{\partial(\rho\ C_p T)}{\partial t} + u_r \frac{\partial}{\partial r}(\rho\ C_p T) + \frac{u_\phi}{r}\frac{\partial}{\partial \phi}(\rho\ C_p T) + u_z \frac{\partial}{\partial z}(\rho\ C_p T) = \frac{1}{r}\frac{\partial}{\partial r}\left\{r\frac{\partial(k\ T)}{\partial r}\right\} + \frac{1}{r^2}\frac{\partial^2(k\ T)}{\partial \phi^2} + \frac{\partial^2(k\ T)}{\partial z^2} + \mu\ \Phi \tag{7}$$

Where Φ is viscous dissipation function.

Fin Equation

Within the fin itself, the energy equation is **(Ramón and Sergio, 2007):**

$$\frac{\partial T}{\partial r} + \frac{T}{r} + \frac{1}{r}\frac{\partial T}{\partial \theta} + \frac{\partial T}{\partial z} = 0 \tag{8}$$

Following **(Aziz and Hellums 1967)** a vorticity vector Ω and a vector potential Ψ with its components:

$$\Psi = \left(\psi_r,\ \psi_\phi,\ \psi_z\right)$$

Defined by:

$$U = \alpha_{eff.}\ \nabla\ \mathrm{X}\ \Psi \tag{9}$$

$$\nabla^2\psi_r = \frac{1}{R}\frac{\partial U_z}{\partial \phi} - \frac{\partial U_\phi}{\partial Z} \tag{10}$$

$$\nabla^2\psi_\phi = \frac{\partial U_r}{\partial Z} - \frac{\partial U_z}{\partial R} \tag{11}$$

$$\nabla^2\psi_Z = \frac{1}{R}\frac{\partial(RU_\phi)}{\partial R} - \frac{1}{R}\frac{\partial U_r}{\partial \phi} \tag{12}$$

Non Dimensional Variables

The characteristic length for the present study is r_2 **(Fukuda et. al.1980)** to convert the governing equations to the dimensionless form, the dimensionless magnitudes must be defined as follow:

$$R = \frac{r}{r_2}, \qquad Z = \frac{z}{r_2}, \qquad U_r = \frac{u_r\, l}{\alpha_m},$$

$$U_\phi = \frac{u_\phi\, l}{\alpha_{eff}}, U_z = \frac{u_z\, l}{\alpha_{eff.}},$$

$$\theta = (T - T_2)/(T_1 - T_2), \quad P = \frac{p\ K\ l}{\alpha_{eff}\ \mu_f\ r_2},$$

,

$$Ra^* = g\ \beta\ K\ (T_1 - T_2)\ (r_2 - r_1)/\alpha_{eff.}\ \upsilon$$

$$S_1 = \frac{s}{2\ r_2},\ S_2 = \frac{\frac{s}{2}+t}{r_2} \quad H_1 = \frac{H_f}{r_2}$$

Substitute these dimensionless magnitudes in the governing equations. Alternative expressions of eq. (3) may be written in terms of $\psi_r,\ \psi_\phi$ *and* ψ_z *as*:

$$U_r = \left(\frac{1}{R}\frac{\partial\psi_z}{\partial\phi} - \frac{\partial\psi_\phi}{\partial Z}\right) \tag{13}$$

$$U_\phi = \left(\frac{\partial\psi_r}{\partial Z} - \frac{\partial\psi_z}{\partial R}\right) \tag{14}$$

$$U_z = \frac{1}{R}\left\{\frac{\partial}{\partial R}\left(R\ \psi_\phi\right) - \frac{\partial\psi_r}{\partial\phi}\right\} \tag{15}$$

Taking curl of momentum equations to eliminate pressure terms, the momentum equations will be:

$$Ra^*\ \frac{l}{(r_2 - r_1)}\left(\frac{1}{R}\sin\delta\frac{\partial\theta}{\partial\phi} + \sin\phi\ \cos\delta\frac{\partial\theta}{\partial Z}\right) =$$
$$-\frac{\partial^2\psi_r}{\partial R^2} - \frac{1}{R^2}\frac{\partial(R\psi_r)}{\partial R} - \frac{2}{R}\frac{\partial\psi_r}{\partial R} - \frac{1}{R^2}\frac{\partial^2\psi_r}{\partial\phi^2}$$
$$-\frac{\partial^2\psi_r}{\partial Z^2} - \frac{2}{R}\frac{\partial\psi_z}{\partial Z} \tag{16}$$

$$Ra^*\ \frac{l}{(r_2 - r_1)}\left(\cos\phi\ \cos\delta\frac{\partial\theta}{\partial Z} - \sin\delta\frac{\partial\theta}{\partial R}\right) =$$
$$-\frac{\partial^2\psi_\phi}{\partial Z^2} - \frac{\partial^2\psi_\phi}{\partial R^2} - \frac{1}{R^2}\frac{\partial^2\psi_\phi}{\partial\phi^2}$$
$$-\frac{2}{R^2}\frac{\partial\psi_r}{\partial\phi} + \frac{\psi_\phi}{R^2} - \frac{1}{R}\frac{\partial\psi_\phi}{\partial R} \tag{17}$$

$$-Ra^*\ \frac{l}{(r_2 - r_1)}\ \cos\delta\left(\frac{1}{R}\cos\phi\frac{\partial\theta}{\partial\phi} + \sin\phi\frac{\partial\theta}{\partial R}\right) =$$
$$-\frac{\partial^2\psi_z}{\partial R^2} - \frac{1}{R}\frac{\partial\psi_z}{\partial R}$$
$$-\frac{1}{R^2}\frac{\partial^2\psi_z}{\partial\phi^2} - \frac{\partial^2\psi_z}{\partial Z^2} \tag{18}$$

The vector potential equation was obtained in the dimensionless form as

$$\nabla^2\psi_r = \frac{\partial^2\psi_r}{\partial R^2} - \frac{1}{R^2}\frac{\partial(R\ \psi_r)}{\partial R}$$
$$-\frac{2}{R}\frac{\partial\psi_r}{\partial R} - \frac{1}{R^2}\frac{\partial^2\psi_r}{\partial\phi^2}$$
$$-\frac{\partial^2\psi_r}{\partial Z^2} - \frac{2}{R}\frac{\partial\psi_z}{\partial Z} \tag{19}$$

$$\nabla^2\psi_\phi = -\frac{\partial^2\psi_\phi}{\partial Z^2} - \frac{\partial^2\psi_\phi}{\partial R^2} - \frac{1}{R^2}\frac{\partial^2\psi_\phi}{\partial\phi^2}$$
$$-\frac{2}{R^2}\frac{\partial\psi_r}{\partial\phi} + \frac{\psi_\phi}{R^2} - \frac{1}{R}\frac{\partial\psi_\phi}{\partial R} \tag{20}$$

$$\nabla^2\psi_z = -\frac{\partial^2\psi_z}{\partial R^2} - \frac{1}{R}\frac{\partial\psi_z}{\partial R}$$
$$-\frac{1}{R^2}\frac{\partial^2\psi_z}{\partial\phi^2} - \frac{\partial^2\psi_z}{\partial Z^2} \tag{21}$$

And the energy equation will be:

$$\left(\frac{1}{R}\frac{\partial\psi_z}{\partial\phi} - \frac{\partial\psi_\phi}{\partial Z}\right)\frac{\partial\theta}{\partial R} + \frac{1}{R}\left(\frac{\partial\psi_r}{\partial Z} - \frac{\partial\psi_z}{\partial R}\right)\frac{\partial\theta}{\partial\phi}$$
$$+\left(\frac{\psi_\phi}{R} + \frac{\partial\psi_\phi}{\partial R} - \frac{1}{R}\frac{\partial\psi_r}{\partial\phi}\right)\frac{\partial\theta}{\partial Z}$$
$$= \frac{l}{r_1}\left[\frac{\partial^2\theta}{\partial R^2} + \frac{1}{R}\frac{\partial\theta}{\partial R} + \frac{1}{R^2}\frac{\partial^2\theta}{\partial\phi^2} + \frac{\partial^2\theta}{\partial Z^2}\right] \tag{22}$$

And fin equation will be:

$$\frac{\partial\theta}{\partial R}+\frac{\theta}{R}+\frac{1}{R}\frac{\partial\theta}{\partial\phi}+\frac{\partial\theta}{\partial Z}=0 \qquad (23)$$

Dimensionless Hydraulic Boundary Conditions

For the vector potential field, the boundary conditions are given as:

$$\frac{1}{R}\frac{\partial}{\partial R}\left(R\psi_r\right)=\psi_\phi=\psi_z=0 \qquad at\ R=R_1,1$$

$$\psi_r=\frac{\partial\psi_\phi}{\partial\phi}=\psi_z=0 \qquad at\ \phi=0,\ \pi$$

$$\psi_r=\psi_\phi=\frac{\partial\psi_z}{\partial Z}=0 \qquad at\ Z=0,\ L$$

And for the fin, the boundary conditions are given as:

$$\frac{1}{R}\frac{\partial}{\partial R}\left(R\,\psi_r\right)=\frac{\partial\psi_\phi}{\partial\phi}=\frac{\partial\psi_Z}{\partial Z}=0$$

On the fin faces which were located on the following planes

(fin base)

At R = R_1 *for* $\phi = 0, \pi$
See **Fig.2**

(fin tip)

At $r = r_1+H_f$ *for* $\phi = 0, \pi$

At S_1 *and* S_2 *for any r and* ϕ

Dimensionless Thermal Boundary Conditions

For the temperature field, the dimensionless thermal boundary conditions are:

$$\theta=1 \qquad at\ R=R_1=r_1/r_2$$

$$\theta=0 \qquad at\ R=R_2=1$$

$$\frac{\partial\theta}{\partial\phi}=0 \qquad at\ \phi=0,\ \pi$$

$$\frac{\partial\theta}{\partial Z}=0 \qquad at\ Z=0,\ L$$

$$at\ R=H_1$$

$$-k_{fin}\frac{\partial\theta}{\partial R}\Big|_{fin}=-k_{eff.}\frac{\partial\theta}{\partial R}\Big|_{medium}$$

$at\ S_1$ $at\ any\ R\ and\ \phi$

$at\ S_2$ $at\ any\ R\ and\ \phi$

$$-k_{fin}\frac{\partial\theta}{\partial Z}\Big|_{fin}=-k_{eff.}\frac{\partial\theta}{\partial Z}\Big|_{medium}$$

$at\ \phi=0,\ \pi$ $and\ any\ R$

$$-k_{fin}\frac{\partial\theta}{\partial\phi}\Big|_{fin}=-k_{eff.}\frac{\partial\theta}{\partial\phi}\Big|_{medium}$$

Where

$$k_{ef}=\left(1-\varepsilon\right)k_s+\varepsilon\,k_f \qquad (24)$$

COMPUTATIONAL TECHNIQUE

Eq. (16, 17, 18, 22 and 23) were transformed into the finite difference equations, where the upwind differential method in the left hand side of the energy eq.(22) and the centered – space differential method for the other terms were used, and solved by using (SOR) method **(Wang and Zhang 1990).** A computer program was built using Fortran 90 language to meet the requirements of the problem.

The value of the vector potential ψ will be calculated at each node, in which the value of vector potential is unknown, the other node

will appear in the right hand side of each equation. As an initial value of iteration, zero is chosen for the vector potential field, while a conduction solution is adopted for temperature field. The index (n) was used to represent the nth – approximation of temperature denoted by θ^n and substituted into the approximated equations, which were solved to obtain the nth approximation of vector potential ψ, then ψ was substituted into eq. (22) to obtain θ^{n+1}. A similar procedure is repeated until the prescribed convergence criterion given by inequality:

$$Max\left|\frac{\theta^{n+1}-\theta^{n}}{\theta^{n}}\right| \le 10^{-8}$$

was established **(Fukuda et. al. 1980).**

It is clear that as the grid becomes finer, the convergence of the results becomes better. The number of grid points used was 21 grid points in the R – direction, 31 in the ϕ – direction and 301 in the Z – direction which seems reasonable and will be used in the present study.

Calculation of Local and Average Nusselt Number

Local Nusselt number is the dimensionless parameter indicative of the rate of energy convection from a surface and can be obtained as follows **(Fukuda et.al. 1980]:**

$$Nu=\frac{q(r_2-r_1)}{k(T_1-T_2)} \qquad (25)$$

The local Nusselt number Nu_1 and Nu_2 on the inner and the outer cylinders are written in the form **(Fukuda et.al. 1980):**

$$Nu_1=-(1-R_1)\left(\frac{\partial\theta}{\partial R}\right)_{R=R_1} \qquad (26)$$

$$Nu_2=-(1-R_1)\left(\frac{\partial\theta}{\partial R}\right)_{R=1_1} \qquad (27)$$

The average Nusselt number Nu_{in} and Nu_{out} on the inner and the outer cylinders are defined as:

$$Nu_{in}=-(1-R_1)\frac{1}{\pi L}\int_0^L\int_0^\pi\left(\frac{\partial\theta}{\partial R}\right)_{R=R} d\phi\, dZ \qquad (28)$$

$$Nu_{out}=-(1-R_1)\frac{1}{\pi L}\int_0^L\int_0^\pi\left(\frac{\partial\theta}{\partial R}\right)_{R=1} d\phi\, dZ \qquad (29)$$

RESULTS AND DISCUSSION

Temperature Field

The dimensionless temperature distribution within the enclosure is presented in a contour map form. One section was selected in the (Z-R) plane along the length of the annulus, and two others in the (R-□) plane in the top and bottom of the annulus, in a manner allowed studying the temperature distribution within each plane.

Fig.3 shows the symmetry of the temperature distribution for horizontal annulus and it was observed that as Rr decrease, isotherms shift towards the outer (cold) cylinder and the waviness will be clear due to the existence of the fins as shown in **Fig.4.** Increase Ra^* and/or decrease in radius ratio results in a thicker cold layer near the bottom wall and a high temperature field near the top wall. More heat is transported upward, and a large difference of temperature is observed between the upper and lower parts of the annulus as shown in **Fig. 5-6**. A reduction in the isotherms observed at the ends of the annulus which was due to the losses of heat transfer by

conduction through the sides (Teflon pieces) and increase as the radius ratio decrease (in other word as the outer radius increase). As Ra^* increase and/or H_f increase, the temperature distribution on the upper boundary gets closer to the temperature distribution predicted for perfectly insulated boundary conditions. Hence the effects of conduction loss through the sides diminish. A swell of the isothermal lines can observed when Ra^* increase which implies a low Nu on the inner cylinder and a high Nu on the outer cylinder. For the same fin length, decreasing fin pitch (in other word increasing the number of fins) cause more shift of the isotherms to the outer cylinder. For vertical annulus the warm region was adjacent to the insulated top wall (see **Fig. 6)** and a decrease of Rr introduce increase in temperature much faster near the hot wall and much slower near the cold wall. This further indicates that the sink temperature for the boundary layer on the hot wall reduces as the curvature effects increase. Also, for low radius ratios, the conduction in the core is very small for any given Ra^*. Previous figures show that for the same H_f and n, increasing the annulus inclination angle from $\delta=0^\circ$ to 60° cause the symmetry of temperature distribution to vanish and an increase in the region of temperature distribution clarify. Since this research was achieved for a steady state laminar region, thus the warm region at the top end when $\delta=90^\circ$ come to be as a concentric circles located at the center of the annulus and distributed between the hot and cold cylinders **Fig. 6.**

When the surface area of the inner cylinder is less than that for outer cylinder and referring to the equation of heat transfer

$$Q = h_i \ A_{in}(T_1 - T_2) = h_o \ A_{out}(T_1 - T_2),$$

h_i will be greater than h_o and owing to this Nu_{in} will be greater than Nu_{out} because the thermal resistance on the inner surface is less than that on the outer one, thus the heat will be transferred to the outer cylinder and the isotherms shift outward. Increasing H_f and decreasing the pitch (i.e. increasing the number of fins) to the limit cause A_{in} to be greater than A_{out}, cause the thermal resistance on the inner surface to be increased causing the heat to be stored in the porous media.

Velocity Fields, Vector Potential and Effect of Inclination

For a horizontal annulus without fins, U_z has constant value along the length of the cylinder for all values of Rr and increasing δ to 30° and 60° cause the existence of unicellular and bicellular flow which cause the velocity to increase and fluid flow toward the top of the annulus. **Fig.7** illustrates a high values of the velocity on the two faces of the fins and on the tip causing the fluid to rise up toward the outer cylinder and decreasing Rr (increasing the outer radius) cause the fluid to cooled before reaching the outer cylinder and its velocity will be reduced. The existence of fins cause the flow to be wavy which in turn enhance the heat transfer toward the outer cylinder but increasing the number of fins or decreasing Rr cause this wavy flow to diminish. The growths of the boundary layers on the vertical wall are also observed to be affected by variation of Rr. The decrease in Rr is seen to reduce the rate of boundary layer growth on the hot wall as shown in **Fig. 8-9.** This behavior is reversed on the cold wall. The net result is a shift of the core toward the top edge of the cooled

wall. This shift is further strengthening if there is an increase in Ra^*. Generally higher convective velocities in the top right – hand corner are produced as a result of the shift. The change in the temperature field brings a noticeable change in the flow patterns as compared to those in vertical annulus as in **Fig.10** for δ = 90 □.

In the (R-□) plane, the radial velocity was not uniform and there exist two cellular; one for negative or low velocity near the outer cylinder and the other for the positive or high velocity near the inner cylinder which move away to the outer cylinder with the decreasing of Rr.

The gravity acceleration vector which aligned with the flow and the density imbalance helps the circulation of the fluid inside the enclosure. When the angle of inclination is zero, the gravity acceleration component aligned with the vertical stream flows is in maximum value, whereas at the horizontal stream flow, the gravity acceleration component is equal zero because it is in the right angle to the flow. As the enclosure inclined in an intermediate angle the gravity acceleration component which is aligned with the stream flow is not zero in all the directions. Therefore, the mass density differences due to the temperature differences of the fluid in all directions can increase the driving force. It is clear that, the influences of increasing the angle of inclination become an increase in the length and/or turn the direction of the streams in a manner of increasing the convection flow.

Fig.11 illustrates for δ =90 □, the regions of high and low velocities in the two sides of each fin which are an indication to the enhancing of heat transfer due to the existence of these fins; as δ increase these regions vanish.

Increasing the number of fins and/ or the length of fins for constant Rr, cause U_r to increase in the region away from the inner cylinder because these fins considered to be a hinder for the movement of the fluid.

Figs. 3-6 show the R – component of the vector potential ψ_r. **Fig.3** illustrates the contour as unicellular of negative value at the center and positive at the boundaries, as the number of fins increase the negative streams abate and the cellular calm down. The same behavior was observed as H_f increased and so was observed as Rr decrease as shown in **Figs. 4-6** and/or as Ra^* decrease as shown in **Fig. 3.**

Figs.12 shows the existence of two regions one of negative stream and another of positive one which extended to the outer cylinder taking larger area as Rr decrease. As δ increase, the stream appear at the bottom of the annulus upper the inner cylinder and another one at the top lower the surface of the inner cylinder extended along the length of the cylinder, its strength increase far away from the surface of the cylinders and its value become zero or negative at the boundaries of the inner and outer cylinders. These Figures show that increasing fin length cause to decrease the strength of the stream.

Effect of Modified Rayleigh number and Other Parameteres

Fig. 13 shows the variation of the average Nusselt number on the hot cylinders with Ra^* for different radius ratios, without and with fins respectively. These figures show that for any radius ratio, the average *Nu* generally constant for low values of Ra^*, this indicate that *Nu* hardly affected by δ for low Ra^*, then as Ra^* reached nearly 100, *Nu* increased with increasing Ra^*. These values increased

as *Rr* decrease due to the enlarge of the distance between the two cylinders. For low values of Ra^* (with or without fins), the maximum values of *Nu* was for maximum *Rr* until Ra^* reached nearly 100, then the situation will inverse and the maximum values of *Nu* would be for minimum *Rr* which improve that for low values of Ra^* the heat transferred by conduction and as Ra^* increased the convection heat transfer would be the dominant. The results show as Ra^* exceed 100, the value of *Nu* increase and as H_f increase *Nu* decrease and decreasing the pitch (by increasing fin numbers) cause *Nu* to decrease. In order to reveal the effect of inclination angle and fin number (which is an indication to fin pitch) on the average Nusselt number, a comparison between the curves in **Fig.14** indicates that there is a reduction in the average Nusselt number with increasing the number of fins and δ, and the maximum heat achieved was for horizontal annulus.

Fig.15 indicates that there is a reduction in the average Nusselt number with increasing H_f from 3mm to 11mm. For the same value of Ra^*, reduction in the average Nusselt number may be ranged between (18% to 38 %).

Local and Average Nusselt Number

Distribution of local Nusselt number along the circumstance of hot and cold cylinders is illustrated in **Fig. 16** at three locations; located at the top of the cylinder, at the center of the cylinder and the third at the bottom of the cylinder. These curves illustrate all the cases with and without fins and for different values of parameters. The local Nusselt number on the cold wall had an increasing trend from ($\phi = 0^\circ$) to ($\phi = 180^\circ$), where the highest values were reached. There were three regions which could be distinguished.

Most of the experimental values were lower than that of the numerical; one of the reasons may be the conduction losses through the top and bottom and hence the absence of perfectly insulated ends boundaries and this is true even by this research or by **(Prasad and Kulacki 1985) and (Havstad and Burns 1982)**

Fig.16 illustrate For horizontal annulus ($\delta = 0^\circ$), attaching fins to the inner cylinder cause the local Nu to be wavy and this wavy phenomenon increased with the increasing of Ra^* and decreased with decreasing the radius ratio and vanish with the increase of the angle of inclination and/or the number of fins, while increasing the fin length cause a disturb of the flow and an increase in the wavy local Nu would be observed.

To the best of the investigator knowledge there is no previous work was found in the literature that studied the effect of annular fins on heat transfer and fluid flow characteristics of buoyancy driven flow in a three dimensional inclined annulus filled with porous media. Therefore, comparison of the present work (case with fins) with that of the literature cannot be achieved. However, the present work of case without fins can be compared with previous works. A comparison for the variation of the average Nusselt number on the inner and outer cylinders with Ra^* was made with that of **(Fukuda et. al. 1980)** in **Fig. 17** and its clear that Nu is constant for low values of Ra^*, until Ra^* equal nearly 100, then Nu will increase with the increasing of Ra^* as presented in this work.

The comparison was made for streamlines and isotherms for the case of natural convection in a horizontal cylindrical annulus filled with porous layer by**(Charrier and Mojtabi 1991)** as shown in **Fig. 18.**

CONCLUSIONS

The following major conclusions can be drawn from the experimental and numerical study:

1- Average Nu number increases with increasing fin length at the same Ra^* and fin number unless the surface area of the inner cylinder exceeds that of the outer cylinder, then the heat will be stored in the porous media.

2- Maximum value of local Nu number increasing with the increase of inclination angle and it may be reached twice the value of that for horizontal cylinder.

3- For all parameters, results showed that the average Nu number increases with an increase in modified Rayleigh number and hardly affected by δ for low values of Ra^*.

4- Increasing Rr cause a clearly increase in average Nusselt number for Ra^* □ 100.

5- The peak of the local Nu on the outer cylinder wall generally appeared at a position of Z=L (at the top) and □ with some deviation from π. while for the inner cylinder the peak appeared at a position of Z=0 (bottom of the cylinder).

REFERENCES

Al-Shahrani D. and Zeitoun O., "Natural Convection in Horizontal Annulus with Attached to Inner Cylinder", Submitted for Publication in Alexandria Engineering Journal, Alexandria, Egept, 2007.

Aziz K. and Hellums J. D., "Numerical Solution of the Three Dimensional Equations of Motion for Laminar Natural Convection", The Physics of Fluids, V0l. 10, No. 2, pp. 314 – 324, 1967

Fukuda K., Takata Y., Hasegawa S., Shimomura H. and Sanokawa K., "Three – Dimensional Natural Convection in a Porous Medium Between Concentric Inclined Cylinders", Proc. 19th Natl Heat Transfer Conf., Vol. HTD – 8, pp. 97 – 103, 1980.

Giampietro Fabbri, "Optimum Cross-Section Design of Internally Finned Tubes Cooled By a Various Fluid", Control Engineering Practice, Vol. 13, pp. 929-938, 2005. www.elsevier.com.

Irfan Anjum Badruddin, Zainal Z. A., Aswatha P. A. and Seetharamu K. N., "Thermal Non-Equilibrium Modeling of Heat Transfer Through Vertical Annulus with Porous Medium", Int. J. Heat and Mass Transfer, Vol. 49, pp. 4955-4965, 2006. www.sciencedirect.com.

Nield D. A. and Bejan A., "Convection in Porous Media", Springer-Verlag, New York, 1999.

Prasad, V. and Kulacki, F. A., "Natural Convection in Porous Media Bounded by Short Concentric Vertical Cylinders", Transaction of ASME, J. of Heat Transfer , Vol. 107, pp. 147-154, February, 1985.

Prasad, V., "Numerical study of Natural Convection in a vertical, Porous Annulus with constant heat flux on the inner wall", Int. J. Heat and Mass Transfer. Vol. 29 No. 6, pp. 841-853, 1986.

Ramón L. F. and Sergio G. M., "Three Dimensional Natural Convection in Finned Cubical Enclosure", Int. J. of Heat and Fluid Flow. Vol. 28, pp. 289-298, 2007.

Taha K Alddoss, Mohammad Alkam and Mohammad Shatrah, "Natural Convection from Horizontal Annulus Partially Filled with a Porous Medium", Int. comm. Heat and Mass Transfer, Vol. 31, No. 3, pp. 441-452, 2004. www.sciencedirect.com.

Wang Bu – Xuan and Zhang Xing, "Natural Convection in Liquid Saturated Porous Media Between Concentric Inclined Cylinders" Int. J. Heat and Mass Transfer Vol. 33. No 5, pp. 827-833, 1990.

NOMENCLATURE

Latin Symbols

Unit	Description	Symbol
kJ/kg □ C	Specific heat at constant pressure	C_p
m/s^2	Acceleration due to gravity	g
m	Fin length	H_f
W/m K	Thermal conductivity of the fluid	k_f
W/m K	Thermal conductivity of the solid	k_s
W/m K	Effective thermal conductivity of the porous media	$K_{eff.}$
m^2	Permeability	K
m	Cylinder length	l
-	Dimensionless cylinder length	L
-	Local Nusselt number on the inner cylinder	Nu_1
-	Local Nusselt number on the outer cylinder	Nu_2
-	Average Nusselt number on the inner cylinder	Nu_{in}
-	Average Nusselt number on the outer cylinder	Nu_{out}
N/m^2	Pressure	p
W	Local heat flux	q
m	Radial coordinate	r
m	Dimensionless radial coordinate	R
-	Modified Rayleigh number	Ra^*
-	Radius ratio	Rr
m	Fin pitch	S
K	Temperature	T
m/s	velocity component in r,□ and z - direction	$u_r, u_□, u_z$
-	Dimensionless velocity component in R, □ and Z direction	U_r, $U_□$, U_z
m	Cartesian coordinate system	x, y, z
-	Dimensionless axial coordinate	Z
	FAI in Fig. 16 means □ (angular direction)	FAI

Greek Symbols

Unit	Description	Symbol
m^2/s	Effective thermal diffusivity	α_{eff}
m^2/s	Medium thermal diffusivity	α_m
1/K	Volumetric thermal expansion coefficient	β
degree	Angle of inclination	δ
-	Dimensionless temperature	θ
-	Vector potential component in R, □ and Z – direction	ψ_r, $\psi_□$, ψ_z

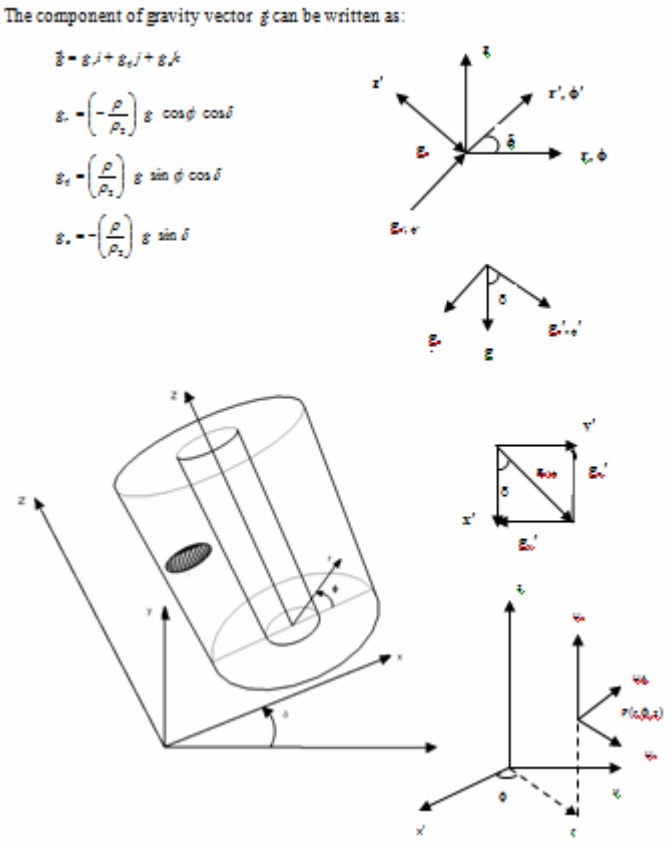

Fig.1 geometry and coordinates system

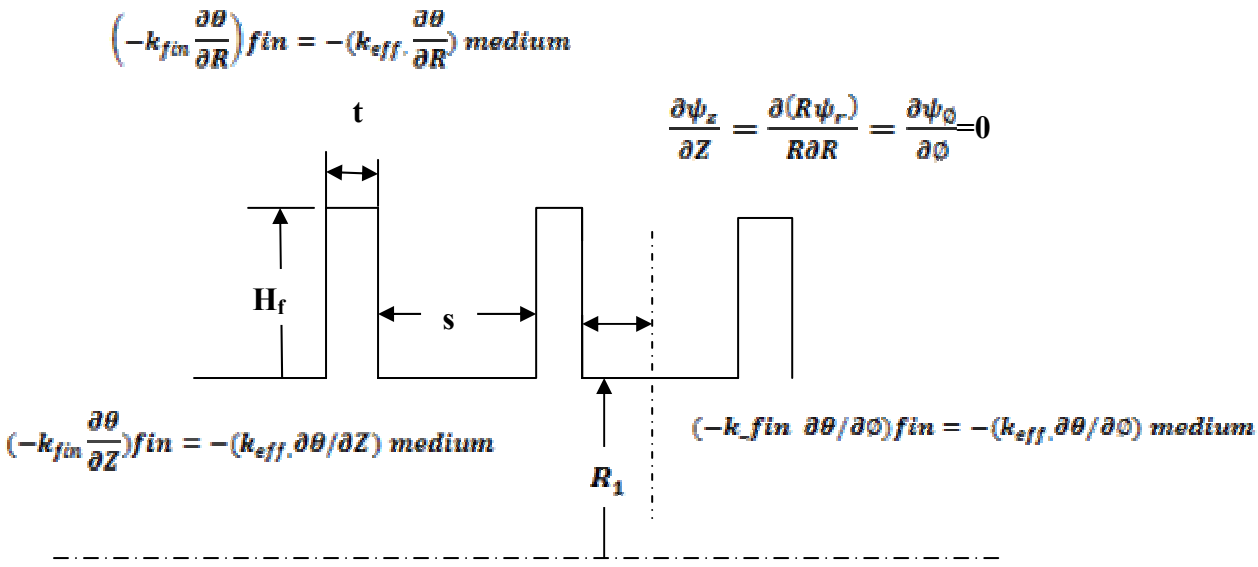

Fig. 2 fin boundary conditions

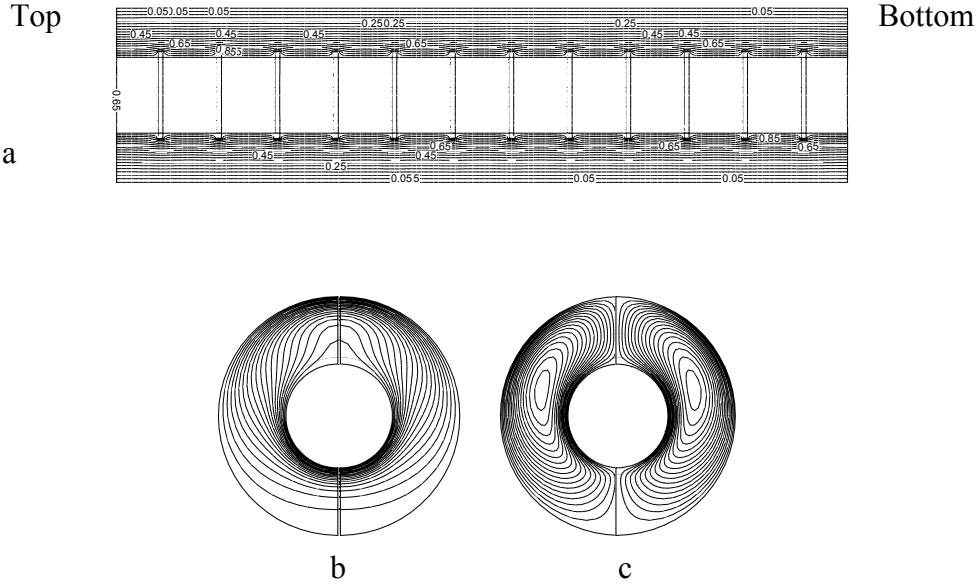

Fig.3 (a) isotherms along the cylinder length (b&c) isotherms and streamlines at the top and bottom sections for Ra^{*}=500,n=12, Rr=0.435, H_f=3mm

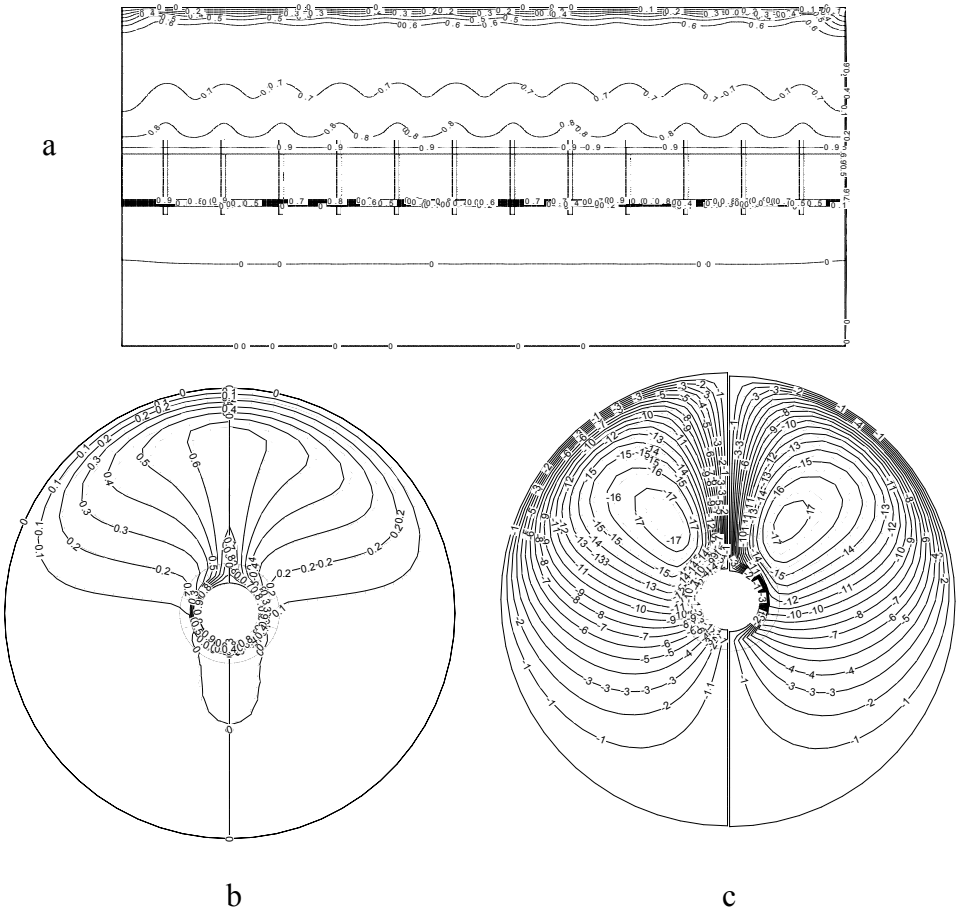

Fig.4 (a) isotherms along the cylinder length (b&c) isotherms and streamlines

at the top and bottom sections for Ra^*=500,n=12, Rr=0.135, H_f=3mm

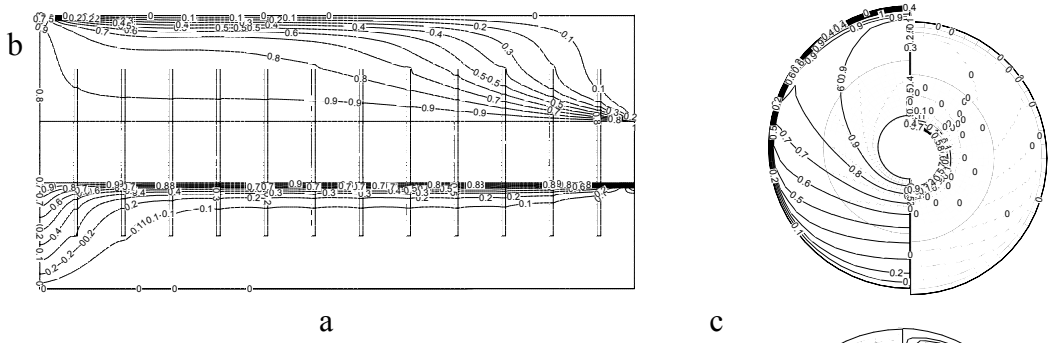

Fig.5 (a) isotherms along the cylinder length (b&c) isotherms and streamlines at the top and bottom sections for Ra^*=500,n=12, Rr=0.225, H_f=11mm,δ=60

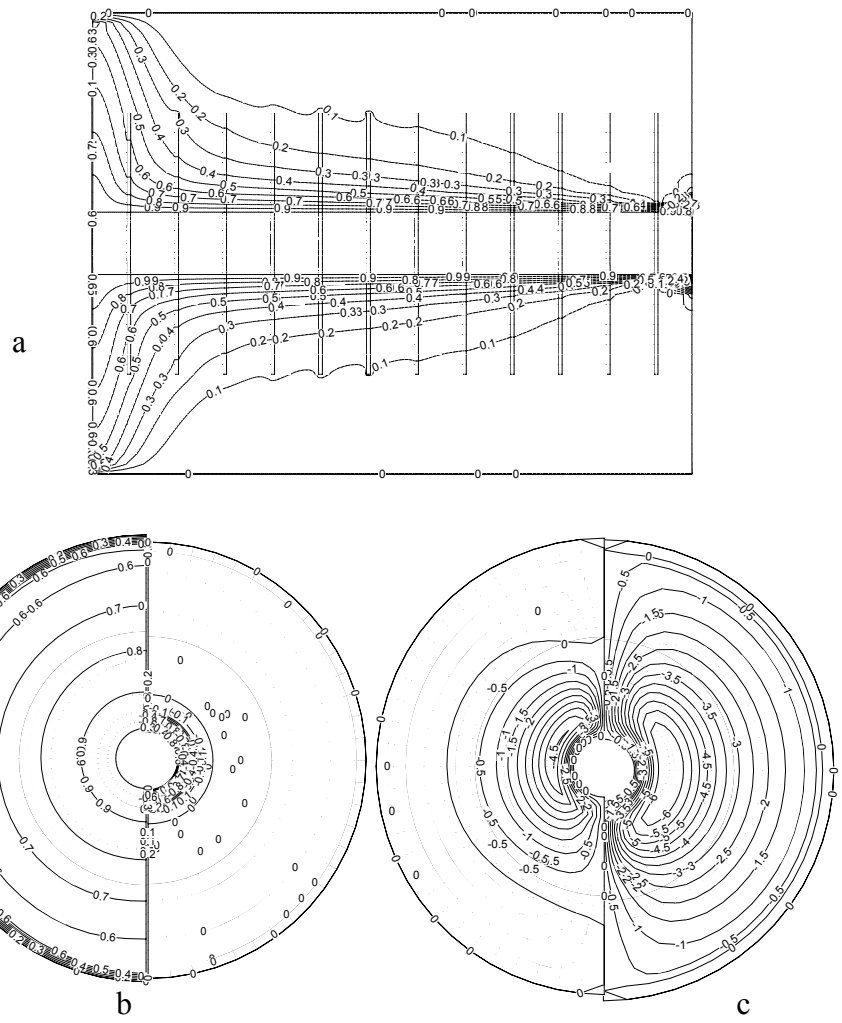

Fig.6 (a) isotherms along the cylinder length (b&c) isotherms and streamlines

at the top and bottom sections for Ra^*=500,n=12, Rr=0.135, H_f=11mm,δ=90□

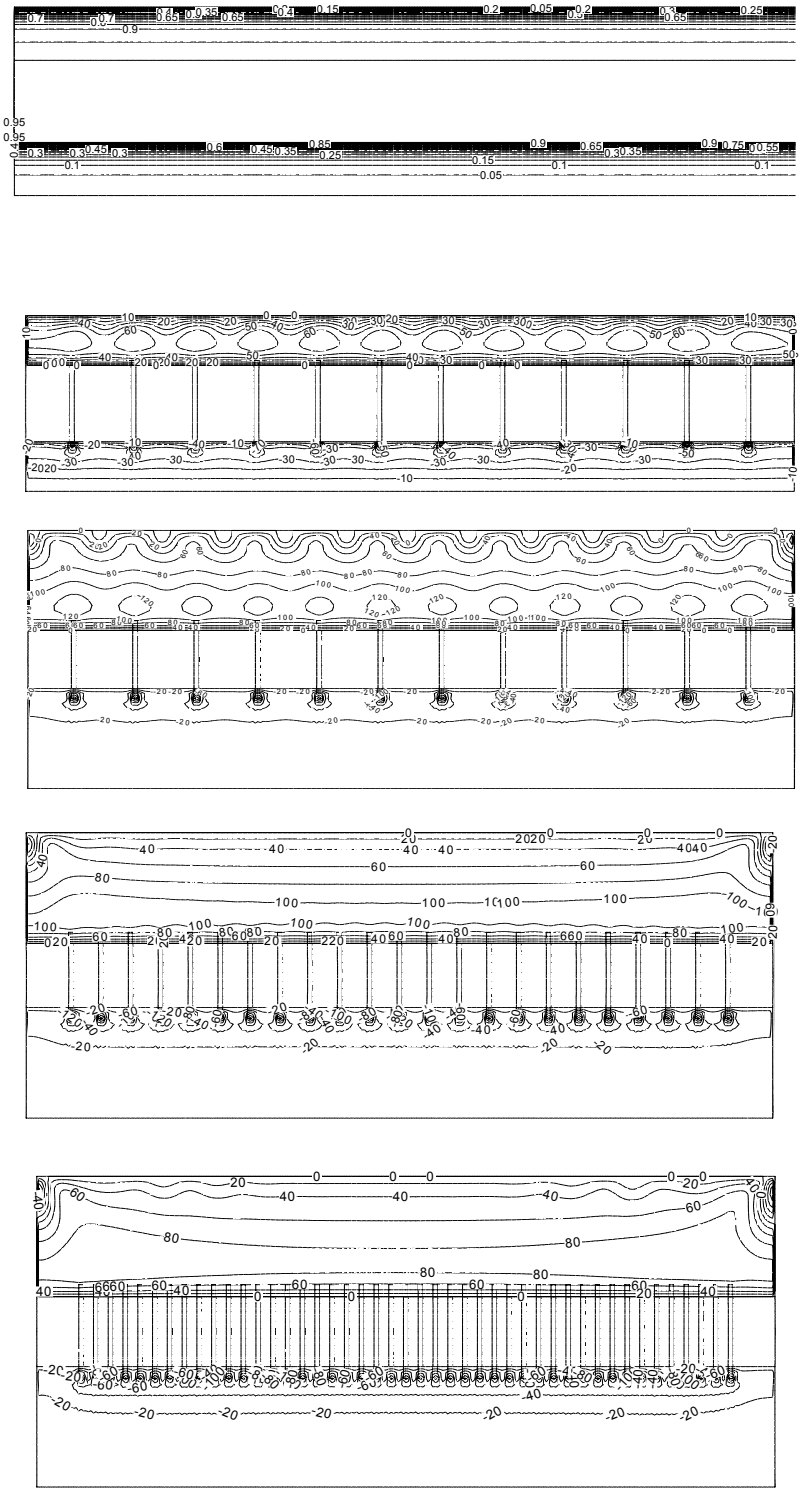

Fig.7 the axial velocity U_z for Ra^*=500,n=0 Rr=0.225, n=12, 23 and 45

H_f=3mm,δ=0°, Rr=0.225 & 0.169 respectively

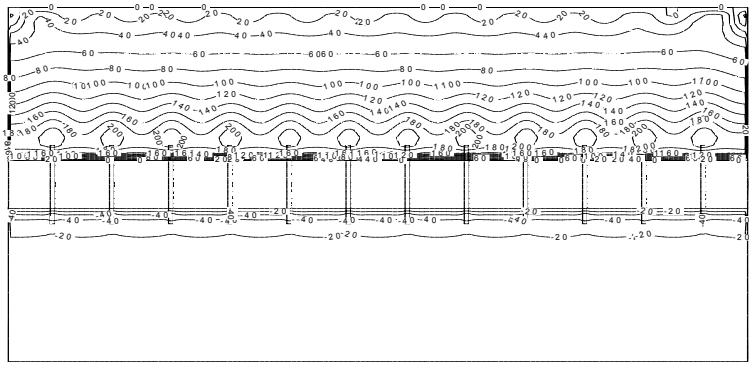

Fig.8 the axial velocity U_z for Ra^*=100,n=12,H_f=3mm,δ=30°, Rr=0.225

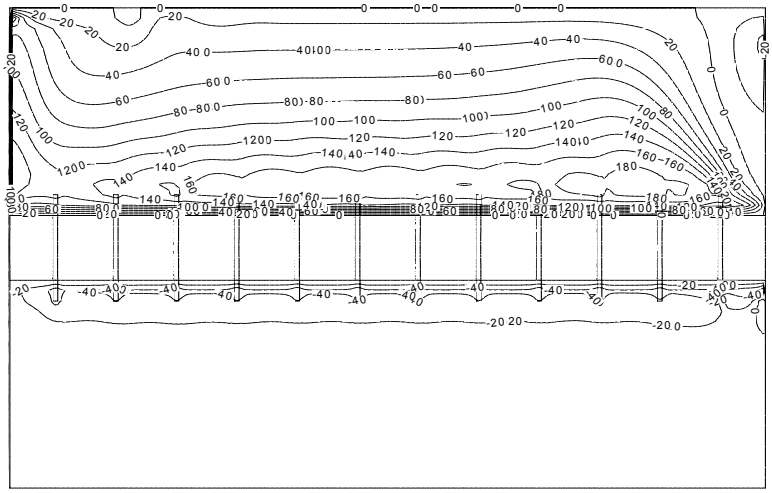

Fig.9 the axial velocity U_z for Ra^*=500,n=12,H_f=3mm,δ=60°, Rr=0.225

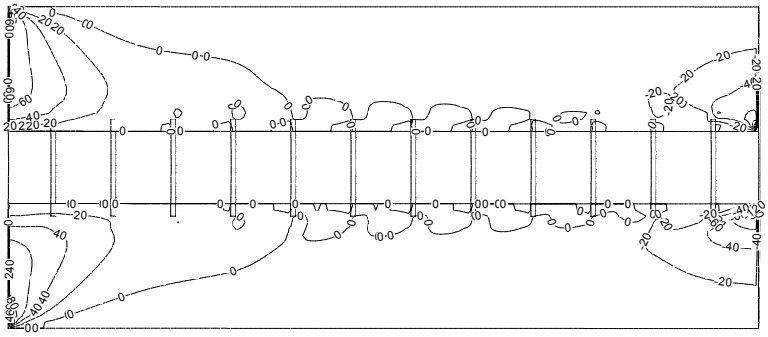

Fig.10 the Axial Velocity U_z for Ra^*=500,n=12,H_f=3mm,δ=90°, Rr=0.225

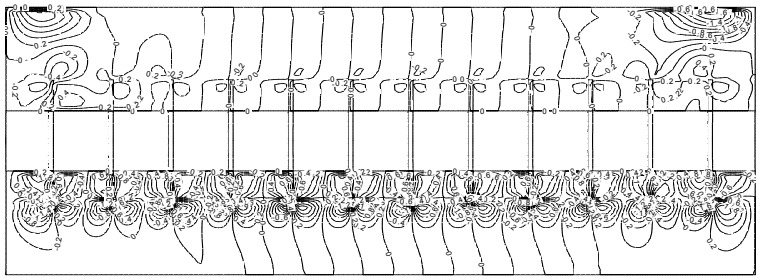

Fig.11 the radial velocity U_r for Ra^*=100,n=12,H_f=7mm,δ=90□,Rr=0.225

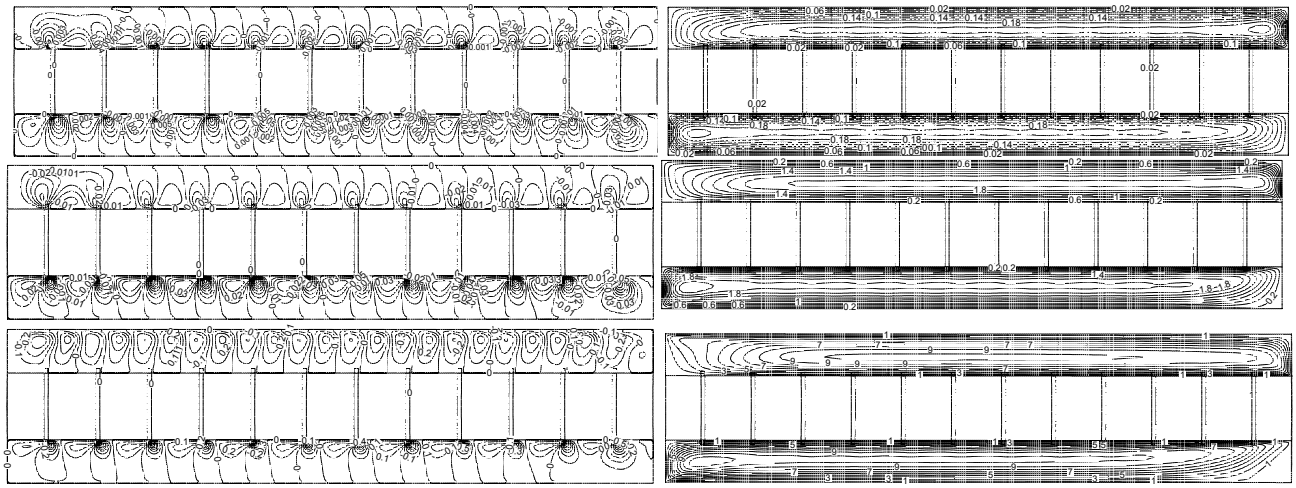

δ=0□ **δ=90□**

Fig. 12 vector potential Ψ_z for n=12, Ra=10,100 and 500 respectively Rr=0.435,Hf=3mm

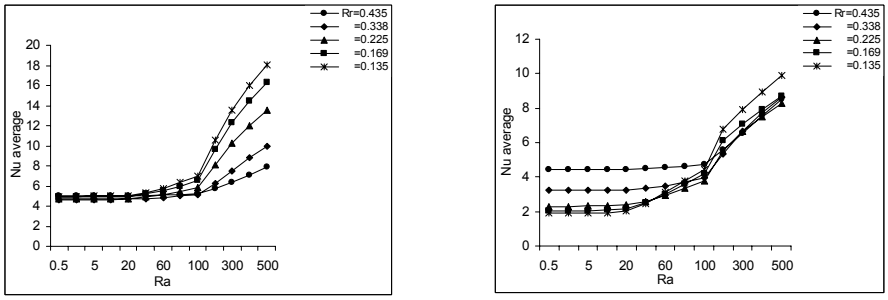

n=0 n=45

Fig.13 the variation of average Nusselt number with Ra^* for different values of Rr

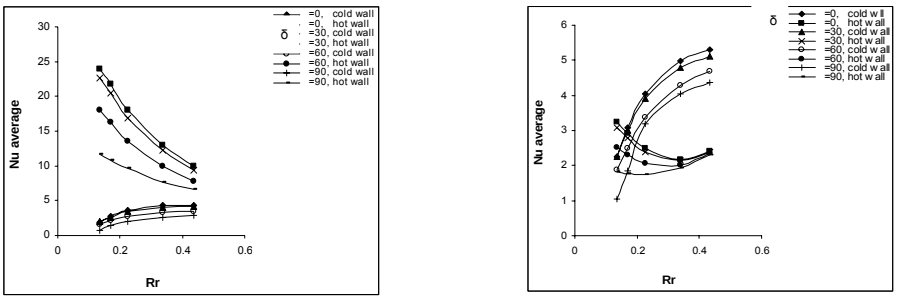

n=0 n=45

Fig.14 the variation of average Nusselt number with radius ratio for different values of inclination angle and number of fins

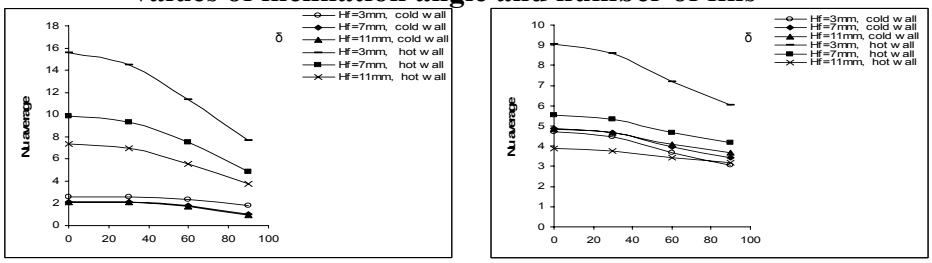

Rr=0.135, Ra=500 n=23 Rr=0.435, Ra=500

Fig.15 variation of average Nu with δ for different H_f, Ra, Rr

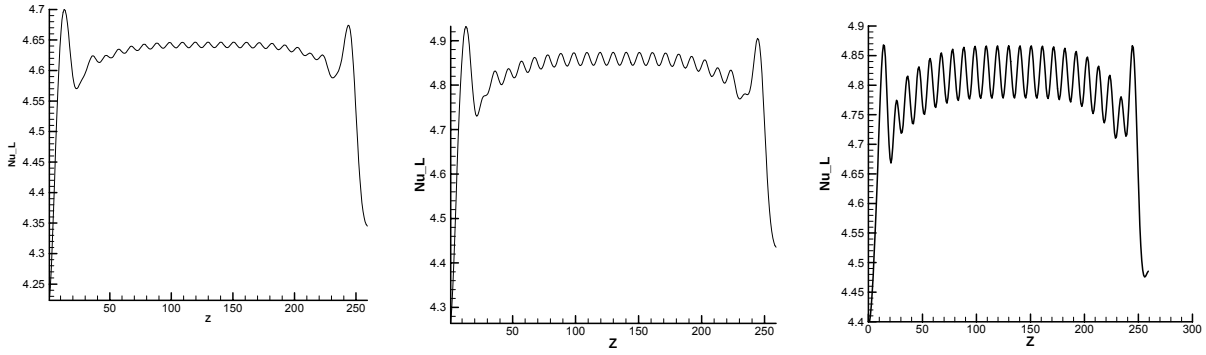

H_f=3mm H_f=7mm H_f=11mm

Fig.16 local Nusselt number along the length of the hot cylinder for n=23,Ra^*=500,Rr=0.435

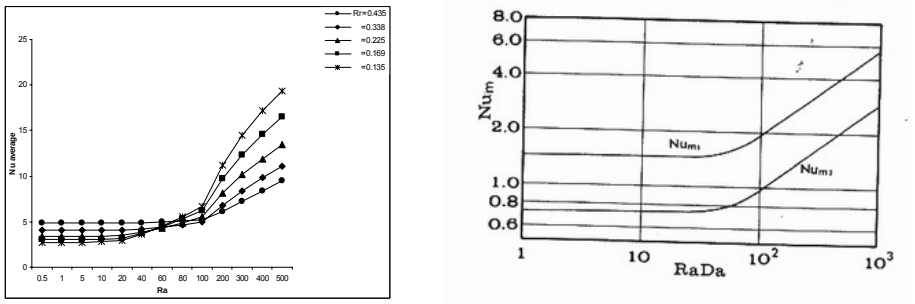

Fig.17 a comparison for the variation of the average Nusselt with Ra^* for the present work with that of [Fukuda and et. al., 1981] respectively

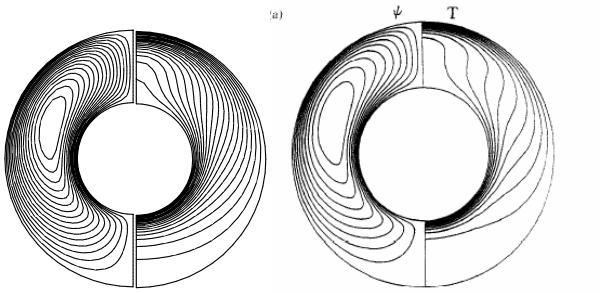

Fig.18 comparison for streamlines and isotherms for the case of convection in a horizontal cylindrical annulus filled with porous media for the present work and by [Charrier and Mojtabi 1991] respectively